24th INTERNATIONAL CONGRESS ON SOUND AND VIBRATION
23–27 July 2017, London

REDUCTION OF AIRCRAFT ENGINE NOISE BY COVERING SURFACE ACOUSTIC METAMATERIALS ON SIDEWALLS

Xiaole Wang and Zhenyu Huang

Shanghai Jiao Tong University, School of Electronic Information and Electrical Engineering, Shanghai, 200240, People's Republic of China
email: bighuang@sjtu.edu.cn

Feng Han and Zixin Feng

Commercial Aircraft Corporation of China Ltd. (COMAC), Shanghai, 201206, People's Republic of China

We propose a surface acoustic metamaterial (SAM) which can be pasted directly on the structure to suppress the sound radiation. As SAM represents great equivalent mass at operating frequencies, the vibration response of the structure decreases significantly. Moreover, SAM can modify the sound radiation characteristics of the structure surface and consequently eliminate the sound radiation efficiency of the structure in working frequencies. In order to control the low-frequency cabin noise arising from the engine vibration and noise, a SAM sample was designed to work at the frequency band of 150-200 Hz with an areal density of 1.28 kg/m^2. The normal incident sound transmission loss of the SAM sample was simulated by using the finite element approach and then validated by experimental measurements in an acoustic impedance tube. Finally, the SAM sample was pasted on the sidewall structure of an aircraft cabin model to investigate the noise control effects. The results showed that the SAM sample can reduce the noise radiation of the sidewall by 10 dB in the frequency range of 160-220 Hz and hence the overall purpose of cabin noise reduction can be achieved.

Keywords: surface acoustic metamaterial, sound radiation efficiency, equivalent mass, sound transmission loss, aircraft cabin noise

1. Introduction

For commercial aircraft in cruise, the engine shaft, turbofan, hydraulic pumps and turbulent boundary layer excitations produce high-level vibration and noise [1]. These vibration and noise energy may transmit through complex structural and air paths into fuselage structures, e.g. skins and stringers, and then radiate noise into the cabin with correlated discrete peaks [2].

The cabin noise control approaches can be roughly classified into passive and active ones. The passive methods require adding conventional noise control materials and structures on the noise and vibration transmission paths. For example, pasting constrained layer damping materials on skins can suppress the bending vibrations and consequently reduce noise radiation [3]; inserting porous materials into the cavity of the sidewall is of utmost importance for improving noise absorption as well as heat insulation performances [4,5]. However, these passive methods cannot effectively reduce the high-level noise peaks in low frequencies, due to the space and weight limits of the aircraft [6-8]. On the other side, the active methods, including active vibration control (AVC) and active noise control (ANC), are much complicated in realization and maintenance [9]. Although AVC and ANC are effective in many cases, they have their own difficult problems to overcome. In general, when applying AVC, a plenty of powerful actuators are required to suppress the widespread vibrations of the radiating structures [10]; and when applying ANC, the effective reduction of low-frequency noise can be achieved only in a small acoustic field [11].

Recently, acoustic metamaterials with deep sub-wavelength scale based on the working mechanism of "locally resonant" have been proposed to possess supernormal vibration suppression [12, 13] sound insulation [14-16] or sound absorption [17-19] capabilities at low frequencies. Many engineering applications in terms of acoustic metamaterials, such as vibration isolators [20, 21] low-frequency acoustic barriers [22, 23], perfect acoustic absorbers [24, 25] and so on are investigated deeply. However, for the aircraft noise reduction, the previous acoustic metamaterials are very difficult to implement due to the strict limits for the overall weight and spatial cost. As the installation space in the cabin sidewall is very small, strong near-field coupling effects between insertion panels and skins cannot be avoided, and consequently result in poor sound insulation performance at low frequencies.

In this paper, we develop a surface acoustic metamaterial (SAM) which consists of locally resonant unit cells with an extreme lightweight construction. SAM is pasted on the surface of a radiation structure, which can not only suppress the bending vibrations of the structure due to the enormous amount of dynamic mass, but also can induce radiation cancellation of the surface due to the anti-phase motions of the sheet in each unit cell at working frequencies.

2. Noise Sources Analysis

For commercial aircraft with engines installed on the rear fuselage, as shown in Fig. 1a, the rear cabin suffers high-level noise from engines. Fig. 1b represents the noise spectrum measured at the rear attendant seat A1 when the aircraft is in cruise with a speed of 0.78 Mach. There are three correlated noise peaks due to engines below 300 Hz, which are the fundamental frequency of engine rotator at 88 Hz and its second- and third- order frequencies at 176 Hz and 264 Hz, respectively.

Transfer-path-analysis indicates that the noise energy at these peaks transmits into the cabin via both the structure-borne and air-borne paths of cabin skins. Hence, the effective way of reducing the cabin noise peaks is to suppress the noise radiation from the skins by pasting SAM with the working frequencies around these peaks. We try to suppress the second order peak because it is more sensitive to human being than the fundamental one and louder than the third one.

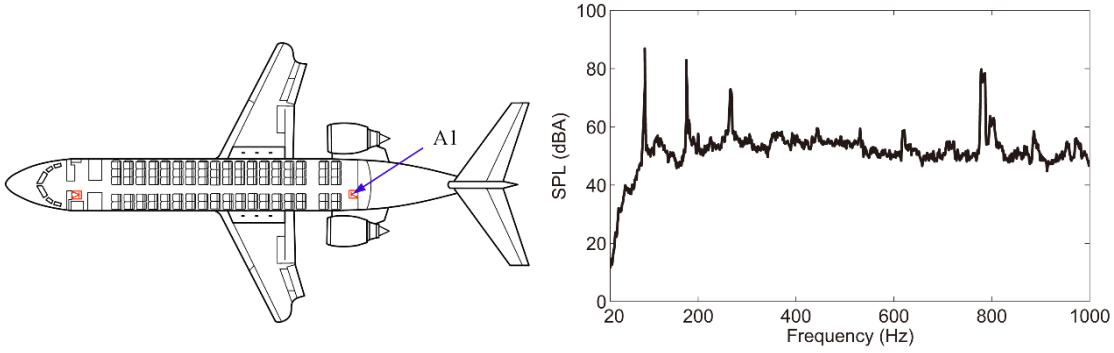

(a) (b)

Figure 1: Rear cabin noise, (a) the schematic diagram of the aircraft and the noise measurement point A1; (b) the noise spectrum of sound pressure level at A1 in cruise.

3. Surface Acoustic Metamaterials

3.1 Structure and Fabrication

SAM unit cells can be pasted individually on the surface of a structure, as shown in Fig. 2a. Each SAM unit cell is composed of a hexagonal support body, a piece of sheet with a hole at the center and an annular mass. The top and bottom surfaces of the support body connects the sheet and the structure surface through glues, respectively; the annular mass is connected on the edge of the hole in the sheet to form a through orifice. In order to facilitate processing, these SAM unit cells can share a continuous piece of sheet for engineering applications, as shown in Fig. 6c (in Section 4).

We fabricated an SAM sample comprising identical unit cells. The geometric dimensions of the unit cell $w_1, w_2, h_1, h_2\ t_1, d_1$ and d_2 (see Fig. 2a) are designed as 16.5 mm, 15 mm, 2 mm, 0.1 mm, 1.3 mm, 8 mm and 12 mm, respectively. The support body, sheet and mass are made of aluminum, Polyimide, and brass, respectively, and the areal density of the proposed SAM sample is 1.28 kg/m^2. Total 31 unit cells are pasted on the aluminum panel with a diameter of 225 mm and a thickness of 1.2 mm by using 3M aerospace sealant (AC-236 B-1/2), as shown in Fig. 2b. We name the whole structure, including the SAM sample and the aluminum panel, as the SAM panel.

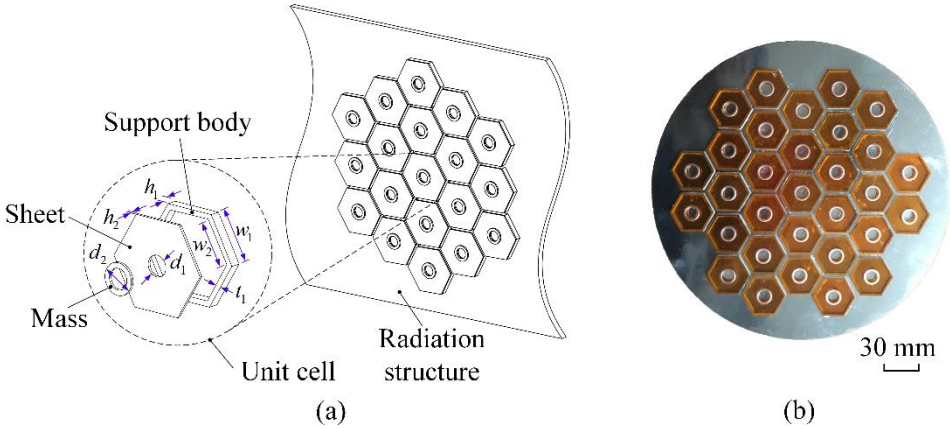

Figure 2: Structure and sample of SAM, (a) the schematic drawing of SAM pasted on the surface of a radiation structure and dimensions of a unit cell; (b) the photograph of the SAM sample.

3.2 Simulation and Experiment

We developed two finite element (FE) models in COMSOL Multiphysics to investigate the sound insulation and sound radiation characteristics of the SAM panel under excitations of the plane wave sound and the point force, respectively. Furthermore, we reveal the working mechanism of SAM by using these FE models.

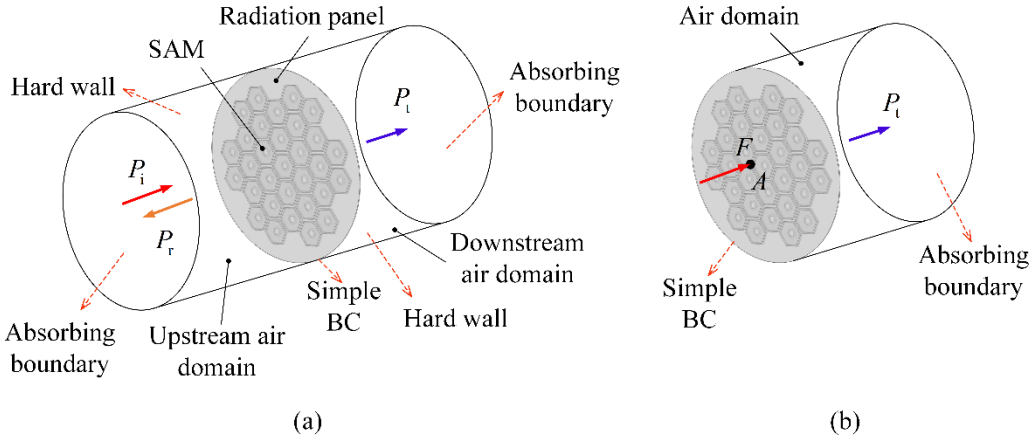

Figure 3: Finite element (FE) models of the SAM panel for calculating sound propagation performances, (a) the FE model of the SAM panel under the excitation of the plane wave sound; (b) the FE model of the SAM panel under the excitation of the point force.

In order to evaluate the normal incident sound transmission loss (STL) of the SAM panel, the upstream and downstream air domains with absorbing boundaries at lateral surfaces and hard wall boundaries at cylindrical surfaces are connected to the fore-surface and rear-surface of the SAM panel, respectively, as shown in Fig. 3a. The boundary condition of the SAM panel is simple-supported and the excitation is the normal incident sound pressure P_i. Meanwhile, by replacing the incident sound

pressure with the point force *F*, the sound radiation characteristics of the SAM panel under the force excitation can be evaluated, as shown in Fig. 3b.

The FE model for calculating STL includes 204,846 tetrahedral elements. The incident sound is a harmonic plane wave with the amplitude of 1 Pa at the fore-surface of the upstream air domain. The normal incidence STL can be calculated as $\mathrm{STL} = 20\log_{10}|P_\mathrm{i}/P_\mathrm{t}|$, where P_i is the incident pressure and P_t is the transmitted one.

This FE model was validated by STL measurements carried out in a large-caliber impedance tube by using the four-microphone method (ASTM E2611-09). The STL comparison between the simulated and measured results of the original aluminum panel and the SAM panel are shown in Fig. 4. It can be found that good agreement between the simulated results and the measured ones is achieved in the frequency band of interest, i.e. 100-300 Hz. Some disagreements nearby the first and second dip frequencies, i.e., 130 Hz and 215 Hz, are due to the inconsistency of the SAM panel. This non-ideal in fabrication processing results in a gentler curve with respect to the measured results than that of the simulated one.

For the aluminum panel and the SAM panel installed in the impedance tube, the first STL dips occur at 120 Hz and 130 Hz, respectively, which is due to the first bending vibration modes of the panels. Considering the modal stiffness increased greater than the modal mass by pasting SAM on the aluminum panel, the first STL dip occurs at the higher frequency domain than that of the aluminum panel. Moreover, very interestingly, based on the simulated results, the STL of the SAM sample is larger than that of the aluminum panel in the frequency range of 130-195 Hz. In particular, the peak value of the SAM panel is almost 14 dB higher than that of the aluminum panel. However, due to the inherent features of the acoustic metamaterials stemmed from the locally resonant mechanism, there is a STL dip occur at 210 Hz.

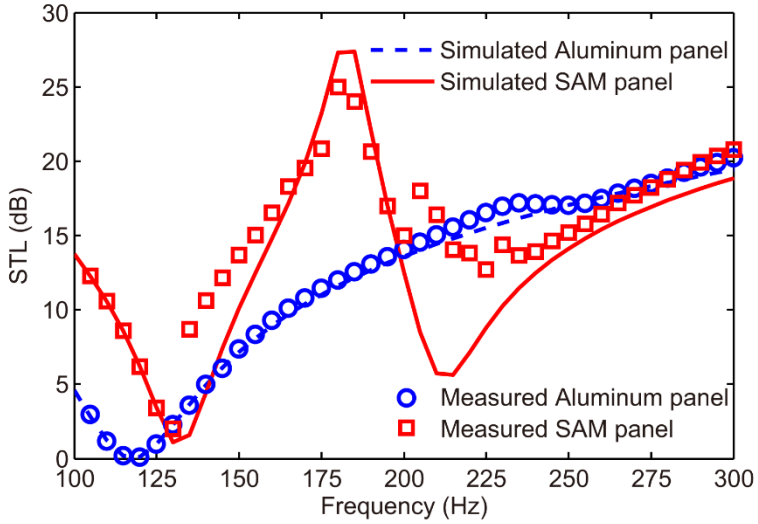

Figure 4: Comparison of STLs of the simulated and measured for the original aluminum panel and the SAM panel, respectively.

The FE model for investigating sound radiation characteristics of the SAM sample includes 204,089 tetrahedral elements. The excitation is a harmonic point force with the amplitude of 1 N applied to the center of the aluminum panel surface. The point with a distance of 20 mm from the surface of the central unit cell of the SAM panel is chosen to be as the observation point at the acoustic near field. Hence, the sound radiation characteristics of the SAM panel can be evaluated by obtaining the frequency response function (FRF) in terms of the pressure response at the observation point and the excited force, denoted as *P*/*F*. We can also readily obtain the other two FRFs which are the driving point accelerance *a*/*F* and the pressure response relative to the acceleration response at the driving point, denoted as *P*/*a*. Where *P*, *F* and *a* represent the sound pressure at the observation point, the excited force and the acceleration at the driving point, respectively. The magnitude of these FRFs are

plotted in Fig. 5, in which the dashed curve represents the aluminum panel and the solid curve represents the SAM panel.

Comparison of the curves shown in Fig. 5a and Fig. 4, the sound-radiation-reduction characteristics by pasting SAM on the aluminum panel is quite similar to the sound-insulation ones. The FRF dip at 177 Hz is consistent with the STL peak frequency. Only the frequency band for effective sound radiation reducing is slightly narrower than that of the STL curve.

Because SAM is attached directly to the structural surface, it can not only suppress the bending vibrations of the structure due to the enormous amount of dynamic mass, but also can induce radiation cancellation of the surface due to the anti-phase motions of the sheet in each unit cell at working frequencies. These two working mechanism can be seen clearly in Fig. 5b and Fig. 5c.

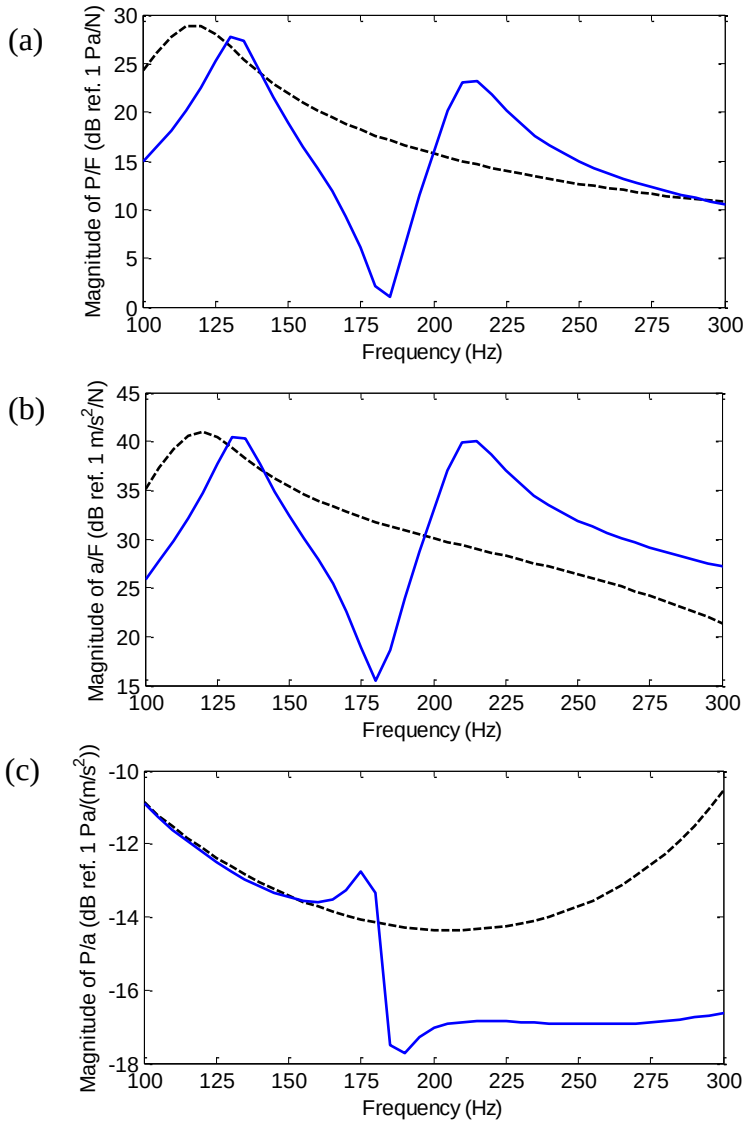

Figure 5: Magnitude of FRFs obtained from the simulation results, the dashed curve represents the aluminum panel and the solid curve represents the SAM panel, (a) Magnitude of *P/F*; (b) Magnitude of *a/F*; (c) Magnitude of *P/a*.

The magnitude of *a*/*F* indicates that how much amount of vibration energy can be suppressed by applied SAM to the aluminum panel. It can be found that the general outline of the curve in Fig. 5b is very similar to the magnitude of *P*/*F* in Fig.5a, which means that the addition-dynamic-mass mechanism plays a more importance role than the radiation-cancellation mechanism in this particular case about SAM. In other works, the SAM sample designed in Section 3.1 acts more like discrete vibration absorbers, when pasted to the aluminum panel. In addition, the uneven surface of the SAM sample

can modify the sound radiation characteristics of the original panel, which may complement the vibration suppression performance and hence to enhance the sound reduction performance of the SAM panel.

4. Application to a Cabin Model

The experimental setup for investigating the sound radiation characteristics of the SAM sample designed in Section 3 consists of a common enclosed room (not a standard reverberation room) and a cabin model, as shown in Fig. 6a. This cabin model is a 1:2 aircraft cabin model with an interior dimeter of 1.6 m and a length of 1.6 m. Seven frames (the ring stiffeners) and twelve stringers (the axial stiffeners) are fixed on the inner skins of the cabin model. The spacing of each adjacent frames and stringers are 0.4 m and 0.38 m, respectively, and the skins, frames and stringers are made of aluminum with thicknesses of 1.5 mm, 10 mm and 2 mm, respectively.

A layer of glass fiber (ORCON P/N 32100332) with a nominal thickness of 1 inch was placed in each area separated by the adjacent frames and stringers, except for the test area as outlined by the white, dashed, lines. The top stringer of the test area was clamped to an end of a shaker (PCB Modal Shop, K2007E01), in which a force sensor (PCB Piezotronics, 208C02) was placed between the excitation point and the stinger of the shaker. The shaker was driven by a white noise input signal with the frequency range of 10-3200 Hz. The sound pressure radiated into the cabin model was measured by using a free-field microphone (BSWA, MA231) located at a near-field observation point which is 20 mm away from the surfaces of the interior test area, as shown in Fig. 6b. Therefore, the FRFs can be measured in terms of the sound pressure of the near-field observation point relative to the input force. In particular, these FRFs have a frequency resolution of 0.5 Hz and are linearly averaged over 100 times.

The FRF correlated to the original surface of the test area toward the inside of the cabin was measured firstly, and then, the SAM sample was pasted on the same surface with a coverage area ratio approximate to be 50%, as shown in Fig. 6c.

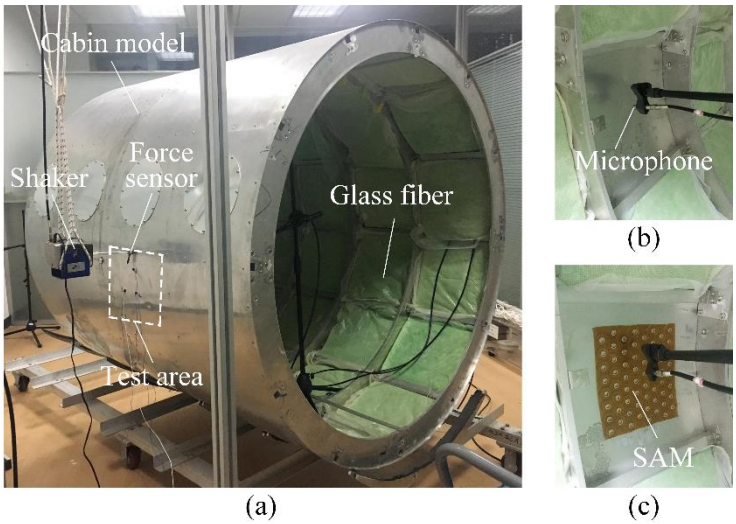

Figure 6: Photograph of the experimental setup, (a) the cabin model; (b) the original surface of the interior sidewall; (c) the SAM surface of the interior sidewall.

Fig.7 illustrates the magnitude of the FRF of the SAM surface compared with that of the original surface. It can be seen that a significant reduction was achieved by pasting the SAM sample to the original surface of the test area at the frequency band of 167-218 Hz. Particularly, at the designed working frequency, i.e., 177 Hz of the SAM sample, the radiated noise into the inner cabin can be suppressed almost 30 dB, when applied the SAM sample to the sidewall of the cabin model. These results validate the effectiveness of the proposed SAM sample for noise reduction applications in the

aircraft. In addition, it is worth noting that the working frequencies of the SAM sample cover some natural frequencies of the skin, thus more effective noise reduction performance of the SAM sample is achieved, comparing with the results obtained from the no-modes analysis discussed in Section 3.2.

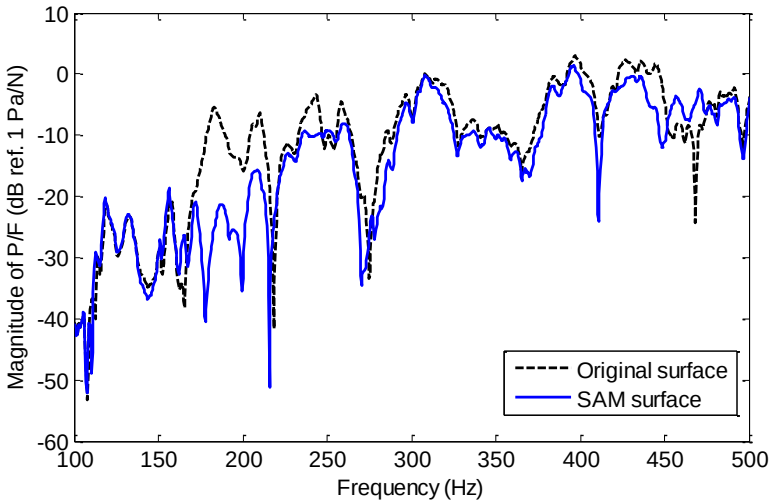

Figure 7: Comparison of the magnitude of FRFs with respect to the original surface (black dashed curve) and the SAM surface (blue solid curve).

5. Conclusion

We proposed a surface acoustic metamaterial for reducing aircraft cabin noise with an extreme lightweight construction. The sound insulation and radiation characteristics of a SAM sample were investigated through simulations and experiments. The results show that, when SAM is pasted on the surface of a radiation structure, it can not only suppress the bending vibrations of the structure due to the enormous amount of dynamic mass, but also can induce radiation cancellation of the surface due to the anti-phase motions of the sheet in each unit cell at desirable working frequencies. These two working mechanism can be designed to complement together to enhance the sound reduction performance and broaden the working frequency band. Finally, we applied the SAM sample to a cabin model and achieved significant noise reduction with a coverage ratio of 50%. In the future work, the proposed SAM may be added damping effects and we expect SAM may substitute conventional damping materials to some extent, especially in the aircraft noise control engineering.

ACKNOWLEDGEMENTS

The authors would like to thank Professor Lin Ji from Shandong University for her helpful comments and suggestions. This work is supported by Fund of Aeronautics Science of China (Grant No. 2014ZF57011).

REFERENCES

1 Herdic, P. C., Houston, B. H., Marcus, M. H., Williams, E. G., and Baz, A. M. The vibro-acoustic response and analysis of a full-scale aircraft fuselage section for interior noise reduction. *Journal of the Acoustical Society of America*, **117**(6), 3667-78. (2005).

2 Wilby, J. F. Aircraft interior noise. *Journal of Sound and Vibration*, **190(**190), 545-564. (1996).

3 Henry, J. K., and Clark, R. L. Active control of sound transmission through a curved panel into a cylindrical enclosure. *Journal of Sound and Vibration*, **249**(2), 325-349. (2002).

4 Holmer, C. I. Approach to interior noise control. I - damped trim panels. *Journal of Aircraft*, **22**(7), 618-623. (1985).

5 Cao, X., Hua, H., and Zhang, Z. Acoustic radiation from stiffened cylindrical shells with constrained layer damping. *Journal of Vibration and Acoustics,* **135**(1), 011005. (2013).

6 Fuller, C. R., Maillard, J. P., Mercadal, M., and Von Flotow, A. H. Control of aircraft interior noise using globally detuned vibration absorbers. *Journal of Sound and Vibration,* **203**(5), 745-761, (1997).

7 Liu, Y., and He, C. On sound transmission through double-walled cylindrical shells lined with poroelastic material: comparison with zhou's results and further effect of external mean flow. *Journal of Sound and Vibration,* **358**, 192-198. (2015).

8 Panneton, R., and Atalla, N. Numerical prediction of sound transmission through finite multilayer systems with poroelastic materials. *Journal of the Acoustical Society of America,* **100**(1), 346-354. (1996).

9 Gardonio, P. Review of active techniques for aerospace vibro-acoustic control. *Journal of Aircraft,* **39**(2), 206-214. (2012).

10 Gardonio, P., and Elliott, S. J. Active control of structure-borne and airborne sound transmission through double panel. *Journal of Aircraft,* **36**(6), 1023-1032. (1999).

11 Griffin, S., Weston, A., and Anderson, J. Adaptive noise cancellation system for low frequency transmission of sound in open fan aircraft. *Shock and Vibration,* **20**(5), 989-1000. (2013).

12 Peng, H., and Pai, P. F. Acoustic metamaterial plates for elastic wave absorption and structural vibration suppression. *International Journal of Mechanical Sciences,* **89**, 350-361. (2014).

13 Claeys, C. C., Sas, P., and Desmet, W. On the acoustic radiation efficiency of local resonance based stop band materials. *Journal of Sound and Vibration,* **333**(14), 3203–3213. (2014).

14 Yang, Z., Mei, J., Yang, M., Chan, N. H., and Sheng, P. Membrane-type acoustic metamaterial with negative dynamic mass. *Physical Review Letters,* **101**(20), 204301. (2010).

15 Yang, Z., Dai, H. M., Chan, N. H., Ma, G. C., and Sheng, P. Acoustic metamaterial panels for sound attenuation in the 50—1000 Hz regime. *Applied Physics Letters,* **96**(4), 1833-21. (2010).

16 Wang, X., Zhao, H., Luo, X., and Huang, Z. Membrane-constrained acoustic metamaterials for low frequency sound insulation. *Applied Physics Letters,* **108**(4), 041905. (2016).

17 Mei, J., Ma, G., Yang, M., Yang, Z., Wen, W., and Sheng, P. Dark acoustic metamaterials as super absorbers for low-frequency sound. *Nature Communications,* **3**(2), 756. (2012).

18 Ma, G., Yang, M., Xiao, S., Yang, Z., and Sheng, P. Acoustic metasurface with hybrid resonances. *Nature Materials,* **13**(9), 873. (2014).

19 Yang, M., Meng, C., Fu, C., Li, Y., Yang, Z., and Sheng, P. Subwavelength total acoustic absorption with degenerate resonators. *Applied Physics Letters,* **107**(10), 153-878. (2015).

20 Yu, D., Wen, J., Shen, H., Xiao, Y., and Wen, X. Propagation of flexural wave in periodic beam on elastic foundations. *Physics Letters A,* **376**(4), 626-630. (2012).

21 Wang, T., Sheng, M. P., Guo, Z. W., and Qin, Q. H. Flexural wave suppression by an acoustic metamaterial plate. *Applied Acoustics,* **114**, 118-124. (2016).

22 Varanasi, S., Bolton, J. S., Siegmund, T. H., and Cipra, R. J. The low frequency performance of metamaterial barriers based on cellular structures. *Applied Acoustics,* **74**(4), 485-495. (2013).

23 Varanasi, S., Bolton, J. S., and Siegmund, T. Experiments on the low frequency barrier characteristics of cellular metamaterial panels in a diffuse sound field. *Journal of the Acoustical Society of America,* **141**(1), 602. (2017).

24 Fu, C., Zhang, X., Yang, M., Xiao, S., and Yang, Z. Hybrid membrane resonators for multiple frequency asymmetric absorption and reflection in large waveguide. *Applied Physics Letters,* **110**(2), 021901. (2017).

25 Long, H., Cheng, Y., Tao, J., and Liu, X. Perfect absorption of low-frequency sound waves by critically coupled subwavelength resonant system. *Applied Physics Letters,* **110**(2), 023502. (2017).